

*Alexander Shashkin, Institute of Solid State Physics, Chernogolovka,  
Moscow District 142432, Russia  
Sergey Kravchenko, Physics Department, Northeastern University, Boston,  
Massachusetts 02115, U.S.A.*

---

*Quantum phase  
transitions in  
two-dimensional electron  
systems*

*CRC PRESS  
Boca Raton Ann Arbor London Tokyo*



---

# *Contents*

<b>1</b>	<b>Quantum phase transitions in two-dimensional electron systems</b>	<b>1</b>
1.1	Strongly and weakly interacting 2D electron systems . . . . .	1
1.2	Proof of the existence of extended states in the Landau levels	3
1.3	Metal-insulator transitions in perpendicular magnetic fields . . . . .	4
1.3.1	Floating-up of the extended states . . . . .	5
1.3.2	Similarity of the insulating phase and quantum Hall phases . . . . .	8
1.3.3	Scaling and thermal broadening . . . . .	11
1.4	Zero-field metal-insulator transition . . . . .	13
1.5	Possible ferromagnetic transition . . . . .	15
1.6	Outlook . . . . .	17
	<b>References</b>	<b>19</b>



# 1

---

## *Quantum phase transitions in two-dimensional electron systems*

---

### 1.1 Strongly and weakly interacting 2D electron systems

Two-dimensional (2D) electron systems are realized when the electrons are free to move in a plane but their motion perpendicular to the plane is quantized in a confining potential well. At low electron densities in such systems, the strongly-interacting limit is reached because the kinetic energy is overwhelmed by the energy of electron-electron interactions. The interaction strength is characterized by the ratio between the Coulomb energy and the Fermi energy,  $r_s^* = E_{ee}/E_F$ . Assuming that the effective electron mass is equal to the band mass, the interaction parameter  $r_s^*$  in the single-valley case reduces to the Wigner-Seitz radius,  $r_s = 1/(\pi n_s)^{1/2} a_B$  and therefore increases as the electron density,  $n_s$ , decreases (here  $a_B$  is the Bohr radius in semiconductor). Possible candidates for the ground state of the system include Wigner crystal characterized by spatial and spin ordering [1], ferromagnetic Fermi liquid with spontaneous spin ordering [2], paramagnetic Fermi liquid [3], etc. In the strongly-interacting limit ( $r_s \gg 1$ ), no analytical theory has been developed to date. According to numeric simulations [4], Wigner crystallization is expected in a very dilute regime, when  $r_s$  reaches approximately 35. The refined numeric simulations [5] have predicted that prior to the crystallization, in the range of the interaction parameter  $25 \leq r_s \leq 35$ , the ground state of the system is a strongly correlated ferromagnetic Fermi liquid. At higher electron densities,  $r_s \sim 1$ , the electron liquid is expected to be paramagnetic, with the effective mass,  $m$ , and Landé  $g$  factor renormalized by interactions. Apart from the ferromagnetic Fermi liquid, other intermediate phases between the Wigner crystal and the paramagnetic Fermi liquid may also exist.

In real 2D electron systems, the inherent disorder leads to a drastic change of the above picture, which significantly complicates the problem. According to the scaling theory of localization [6], all electrons in a disordered infinite noninteracting 2D system become localized at zero temperature and zero magnetic field. At finite temperatures, regimes of strong and weak localizations are distinguished: (i) if the conductivity of the 2D electron layer is activated, the resistivity diverges exponentially as  $T \rightarrow 0$ ; and (ii) in the opposite limit

of weak localization the resistivity increases logarithmically with decreasing temperature — an effect originating from the increased probability of electron backscattering from impurities to the starting point. Interestingly, the incorporation of weak interactions ( $r_s < 1$ ) between the electrons promotes the localization [7]. However, for weak disorder and  $r_s \geq 1$  a possible metallic ground state was predicted [8].

In view of the competition between the interactions and disorder, high- and low-disorder limits can be considered. In highly-disordered electron systems, the range of low densities is not accessible as the strong (Anderson) localization sets in. This corresponds to the weakly-interacting limit in which an insulating ground state is expected. The case of low-disordered electron systems is much more interesting because low electron densities corresponding to the strongly-interacting limit become accessible. According to the renormalization group analysis for multi-valley 2D systems [9], the strong electron-electron interactions can stabilize the metallic ground state, leading to the existence of a metal-insulator transition in zero magnetic field.

In quantizing magnetic fields, the interaction strength is characterized by the ratio between the Coulomb energy and the cyclotron splitting. In the ultra quantum limit, it is similar to the interaction parameter  $r_s^*$ . Within the concept of single-parameter scaling for noninteracting 2D electrons [10], there is only one extended state in the Landau level, and the localization length diverges at the center of the Landau level [11]. For consistency with the scaling theory of localization in zero magnetic field, it was predicted that the extended states in the Landau levels cannot disappear discontinuously with decreasing magnetic field but must float up indefinitely in energy in the limit of  $B \rightarrow 0$  [12]. The corresponding phase diagram plotted in disorder versus inverse filling factor ( $1/\nu = eB/hcn_s$ ) plane is known as the global phase diagram for the quantum Hall effect [13]. As long as no merging of the extended states was considered to occur, their piercing of the Fermi level was predicted to cause quantization of the Hall conductivity in weak magnetic fields [14]. The case of strongly interacting 2D electrons in the quantum Hall regime has not been considered theoretically. In the very dilute regime, there are theoretical predictions that Wigner crystallization is promoted in the presence of a magnetic field (see, e.g., Ref. [15]).

In this chapter, attention is focused on experimental results obtained in low-disordered strongly interacting 2D electron systems, in particular, (100)-silicon metal-oxide-semiconductor field-effect transistors (MOSFETs). Due to the relatively large effective mass, relatively small dielectric constant, and the presence of two valleys in the spectrum, the interaction parameter in silicon MOSFETs is an order of magnitude bigger at the same electron density than that in the 2D electron system in GaAs/AlGaAs heterostructures. Except at very low electron densities, the latter electron system can be considered weakly interacting. It is worth noting that the observed effects of strong electron-electron interactions are more pronounced in silicon MOSFETs compared to GaAs/AlGaAs heterostructures, although the fractional quantum Hall effect,

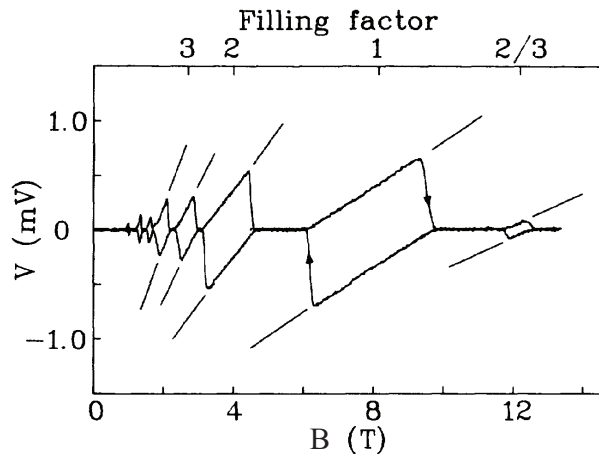
which is usually attributed to electron-electron interactions, has not been reliably established in silicon MOSFETs.

---

## 1.2 Proof of the existence of extended states in the Landau levels

In a magnetically quantized 2D electron system, the Landau levels bend up at the sample edges due to the confining potential, and edge channels are formed where these intersect the Fermi energy (see, e.g., Ref. [16]). There rises a natural question whether the current in the quantum Hall state (in which the Hall resistivity,  $\rho_{xy} = h/\nu e^2$ , is quantized at integer filling factor  $\nu$  accompanied with vanishing longitudinal resistivity,  $\rho_{xx}$  [17]) flows in the bulk or at the edges of the sample. Although the Hall conductivity  $\sigma_{xy}$  was not directly measured in early experiments on the quantum Hall effect, it seemed obvious that this value corresponds to the Hall resistivity  $\rho_{xy}$ , in agreement with the concept of currents that flow in the bulk [18]; that stands to reason that finite  $\sigma_{xy}$  would give evidence for the existence of extended states in the Landau levels [16, 19]. This concept was challenged by the edge current model [20]. In the latter approach extended states in the bulk are not crucial and the problem of current distributions in the quantum Hall effect is reduced to a one-dimensional task in terms of transmission and reflection coefficients as defined by the backscattering current at the Fermi level between the edges. Importantly, if the edge current contributes significantly to the net current, conductivity/resistivity tensor inversion is not justified, because the conductivities  $\sigma_{xx}$  and  $\sigma_{xy}$  are related to the bulk of the 2D electron system. That is to say, a possible shunting effect of the edge currents in the Hall bar geometry makes it impossible to extract the value  $\sigma_{xy}$  from the magnetotransport data for  $\rho_{xx}$  and  $\rho_{xy}$ .

To verify whether or not the Hall conductivity is quantized, direct measurements of  $\sigma_{xy}$  are necessary excluding the shunting effect of the edge currents. Being equivalent to Laughlin's gedanken experiment [21], such measurements were realized using the Corbino geometry which allows separation of the bulk contribution to the net current (see, e.g., Ref. [22]). A Hall charge transfer below the Fermi level between the coasts of a Corbino sample is induced by magnetic field sweep through the generated azimuthal electric field. If the dissipative conductivity  $\sigma_{xx} \rightarrow 0$ , no discharge occurs allowing determination of the transferred charge,  $Q = \sigma_{xy} \pi r_{\text{eff}}^2 c^{-1} \delta B$ , where  $r_{\text{eff}}$  is the effective radius. The induced voltage,  $V = Q/C$ , which is restricted due to a large shunting capacitance,  $C$ , changes linearly with magnetic field with a slope determined by  $\sigma_{xy}$  in the quantum Hall states until the dissipationless quantum Hall state breaks down (Fig. 1.1). The fact that the quantization accuracy of  $\sigma_{xy}$  (about

**FIGURE 1.1**

The induced voltage in a Corbino sample of a GaAs/AlGaAs heterostructure in up- and down-sweeps of the magnetic field. Also shown by straight lines are the expected slopes for  $\nu = 2/3, 1, 2, 3,$  and  $4$ . From Ref. [22].

1%) is worse compared to that of  $\rho_{xy}$  may be attributed to non-constancy of the effective area in not very homogeneous samples. Thus, the Hall current in the quantum Hall effect flows not only at the edges but also in the bulk of the 2D electron system through the extended states in the filled Landau levels.

The finite Hall conductivity measured in the Corbino geometry in the arrangement of Laughlin's gedanken experiment establishes the existence of extended states in the Landau levels for both strongly and weakly interacting 2D electron systems. Note that the insignificance of edge channel effects in transport experiments is verified in a usual way by coincidence of the results obtained in Hall bar and Corbino geometries.

---

### 1.3 Metal-insulator transitions in perpendicular magnetic fields

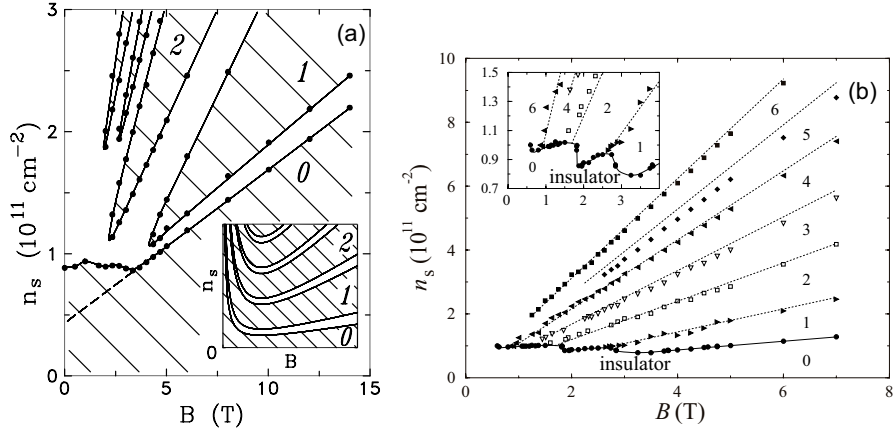
Metal-insulator transitions were studied for the quantum Hall phases and the insulating phase at low electron densities. The insulating phase was attributed to possible formation of a pinned Wigner crystal [23, 24, 25]. However, floating-up of the extended states relative to the Landau level centers and a close similarity of all insulating phases have been found experimentally [26, 27, 28]. Thus, the experimental results excluded the formation of

a pinned Wigner crystal in available samples, but supported the existence of a metallic state in zero field. It was also found that the bandwidth of the extended states in the Landau levels is finite, which is in contradiction to scaling arguments. Strangely, the latter experimental result has not attracted much of the theorists' attention.

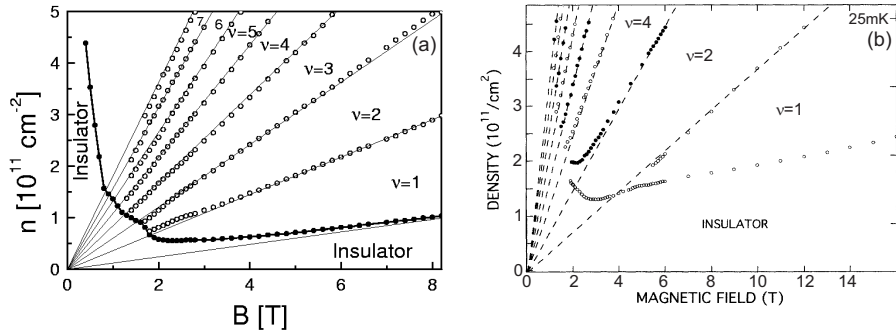
### 1.3.1 Floating-up of the extended states

The first experimental results on the metal-insulator phase diagram at low temperatures in low-disordered silicon MOSFETs [26] already revealed discrepancies with the theory (Fig. 1.2(a)). In that paper, a somewhat arbitrary criterion for the longitudinal conductivity,  $\sigma_{xx} = e^2/20h$ , was used to map out the phase boundary that corresponds to the Anderson transition to the regime of strong localization. However, firstly, the phase boundary was shown to be insensitive to the choice of the cutoff value (see, e.g., Ref. [29]), and secondly, that particular cutoff value is consistent with the results obtained for quantum Hall states by a vanishing activation energy combined with a vanishing nonlinearity of current-voltage characteristics when extrapolated from the insulating phase [27] (note that for the lowest-density phase boundary, a lower value  $\sigma_{xx}^{-1} \approx 100$  kOhm at a temperature  $\approx 25$  mK follows from the latter method). The metallic phase surrounds each insulating phase as characterized by the dimensionless Hall conductivity,  $\sigma_{xy}h/e^2$ , that counts the number of quantum levels below the Fermi level (in bivalley (100)-silicon MOSFETs, spin and valley degeneracies of the Landau level should be taken into account). This indicates that the extended states indeed do not disappear discontinuously. Instead, with decreasing magnetic field they float up in energy relative to the Landau level centers and merge forming a metallic state in the limit of  $B = 0$  (for more on this, see section 1.4). This contradicts the theoretical scenario that in the limit of zero magnetic field the extended states should float up indefinitely in energy [12] leading to an insulating ground state. Besides, the experimental phase boundary at low electron densities oscillates as a function of  $B$  with minima corresponding to integer filling factors. The phase boundary oscillations manifest themselves in that at electron densities near the  $B = 0$  metal-insulator transition, the magnetoresistance oscillates with an amplitude that diverges as  $T \rightarrow 0$  [24]; the regions in which the magnetoresistance diverges are referred to as reentrant insulating phase.

The topology of the observed metal-insulator phase diagram — merging of the extended states and, hence, the presence of direct transitions between the insulating phase with  $\sigma_{xy} = 0$  and quantum Hall phases with  $\sigma_{xy}h/e^2 > 1$  — is robust being insensitive to the method for spotting the phase boundary [27, 30] and to the choice of 2D carrier system [31]. It was verified using a criterion of vanishing activation energy and vanishing nonlinearity of current-voltage characteristics as extrapolated from the insulating phase, which allows more accurate determination of the Anderson transition [27]. A method that had been suggested in Ref. [32] was also applied for similar silicon MOSFETs

**FIGURE 1.2**

(a) Metal-insulator phase diagram in a low-disordered 2D electron system in silicon MOSFETs obtained using a cutoff criterion,  $\sigma_{xx} = e^2/20h$ , at a temperature  $\approx 25$  mK. The dimensionless  $\sigma_{xy}h/e^2$  in different insulating phases is indicated. The slope of the dashed line is close to  $e/2hc$ . A sketch of the expected phase diagram is displayed in the inset. From Ref. [26]. (b) The map of extended states determined by maxima in  $\sigma_{xx}$  in a low-disordered silicon MOSFET. Numbers show  $\sigma_{xy}$  in units of  $e^2/h$ . From Ref. [30].

**FIGURE 1.3**

(a) A map of the extended states for a highly-disordered 2D hole system in a Ge/SiGe quantum well. The open circles represent maxima in  $\rho_{xx}$  and/or  $d\rho_{xy}/dB$ . The solid circles correspond to crossing points of  $\rho_{xx}$  at different temperatures. Numbers show the value of  $\sigma_{xy}h/e^2$ . Adapted from Ref. [31]. (b) Behavior of the extended states determined by maxima in  $\sigma_{xx}$  in a strongly-disordered 2D electron system in GaAs/AlGaAs heterostructures. Numbers show  $\sigma_{xy}$  in units of  $e^2/h$ . Adapted from Ref. [32].

[30]. The extended states were studied by tracing maxima in the longitudinal conductivity in the  $(B, n_s)$  plane (Fig. 1.2(b)) and good agreement with the aforementioned results was found. A similar merging of at least the two lowest extended states was observed in a more-disordered 2D hole system in a Ge/SiGe quantum well [31] (Fig. 1.3(a)). The extended states were associated either with maxima in  $\rho_{xx}$  and/or  $d\rho_{xy}/dB$ , or with crossing points of  $\rho_{xx}$  at different temperatures. It is noteworthy that a bad combination of the criterion for determining the phase boundary and the 2D carrier system under study may lead to a failure of mapping out the phase diagram down to relatively weak magnetic fields. In Ref. [32], extended states were studied by measuring maxima in the longitudinal conductivity in the  $(B, n_s)$  plane for the strongly-disordered 2D electron system in GaAs/AlGaAs heterostructures (Fig. 1.3(b)). Because of strong damping of the Shubnikov-de Haas oscillations in low magnetic fields, the desired region on the phase diagram below 2 T was not accessible in that experiment. This invalidates the claim of Glozman *et al.* [32] that the extended states do not merge. The behavior of the lowest extended state in Fig. 1.3(b), which Glozman *et al.* [32] claim to float up above the Fermi level as  $B \rightarrow 0$ , simply reflects the occurrence of a phase boundary oscillation minimum at filling factor  $\nu = 2$ , similar to both the minimum at  $\nu = 1$  in Fig. 1.3(a) and to the case of silicon MOSFETs (Fig. 1.2). Such a minimum manifests itself in that there exists a minimum in  $\rho_{xx}$  at integer  $\nu \geq 1$  that is straddled by the insulating phase. To this end, all available data for the metal-insulator phase diagrams agree well with each other, except those in the vicinity of  $B = 0$ . In weak magnetic fields, experimental results obtained in 2D electron systems with high disorder are not method-independent. Glozman *et al.* [32] found that the cutoff criterion yields basically a flat phase boundary towards  $B = 0$ , which is in agreement with the data for silicon MOSFETs (Fig. 1.2(a)). On the contrary, Hilke *et al.* [31] employed the method based on temperature dependences of  $\rho_{xx}$  and obtained a turn up on the phase boundary in Fig. 1.3(a). Note that the validity of the data for the lowest extended state at magnetic fields  $\leq 1.5$  T in Fig. 1.3(a) is questionable because the weak temperature dependences of  $\rho_{xx}$  as analyzed by Hilke *et al.* [31] cannot be related to either an insulator or a metal.

As a matter of fact, the weak-field problem — whether or not there is an indefinite rise of the phase boundary as  $B \rightarrow 0$  — is a problem of the existence of a metal-insulator transition at  $B = 0$  and  $T = 0$ . In dilute 2D electron systems with low enough disorder, the resistivity,  $\rho$ , strongly drops with lowering temperature [33, 34] providing an independent way of facing the issue. Given strong temperature dependences of  $\rho$ , those with  $d\rho/dT > 0$  ( $d\rho/dT < 0$ ) can be associated with a metallic (insulating) phase [33, 34]. If extrapolation of the temperature dependences of  $\rho$  to  $T = 0$  is valid, the curve with  $d\rho/dT = 0$  should correspond to the metal-insulator transition (see section 1.4). As long as in more-disordered 2D carrier systems the metallic ( $d\rho/dT > 0$ ) behavior is suppressed (see, e.g., Refs. [35, 36]) or disappears entirely, it is definitely

incorrect to extrapolate those weak temperature dependences of  $\rho$  to  $T = 0$  with the aim to distinguish between insulator and metal.

Another point to compare experiment and theory is the oscillating behavior of the phase boundary that restricts the insulating phase with  $\sigma_{xy} = 0$  (see, e.g., Fig. 1.2). Note that the oscillations persist down to the magnetic fields corresponding to the fillings of more than one Landau levels. The oscillation period includes the following stages. With decreasing magnetic field the lowest extended states follow the Landau level, float up in energy relative to its center, and merge with extended states in the next quantum level. No merging was present in the original theoretical considerations [12, 13, 14] leading to discrepancies between experiment and theory. Recently, theoretical efforts have been concentrated on modifications of the global phase diagram for the quantum Hall effect to reach topological compatibility with the observed metal-insulator phase diagram. Although floating and/or merging of the extended states can be obtained in the calculations, the oscillations of the phase boundary at low electron densities have not yet been described theoretically.

### 1.3.2 Similarity of the insulating phase and quantum Hall phases

The insulating phase at low electron densities was considered to be a possible candidate for a pinned Wigner crystal. It was argued that its aforementioned reentrant behavior is a consequence of the competition between the quantum Hall effect and the pinned Wigner crystal [24]. Another argument was strongly nonlinear current-voltage characteristics in the insulating phase which were attributed to depinning of the Wigner crystal. Similar features of the insulating phase in a 2D electron (near  $\nu = 1/5$ ) [23] and 2D hole (near  $\nu = 1/3$ ) [25] systems in GaAs/AlGaAs heterostructures with relatively low disorder were also attributed to a pinned Wigner crystal which is interrupted by the fractional quantum Hall state. An alternative scenario was discussed in terms of percolation metal-insulator transition [29, 37, 38]. To distinguish between the two scenarios, the behavior of activation energy and current-voltage characteristics in the insulating phase was studied and compared to that in quantum Hall phases [27, 28].

In contrast to the low-density insulating phase, the way of determining the current-voltage characteristics of the quantum Hall phases is different for Corbino and Hall bar geometries. In the former the dissipationless Hall current does not contribute to the dissipative current that is proportional to  $\sigma_{xx}$ , allowing straightforward measurements of current-voltage curves for all insulating phases. In the latter the two current channels are connected through edge channels (see section 1.2), and current-voltage characteristics correspond to quantum-Hall-effect breakdown curves. The dissipative backscattering current,  $I$ , that flows between opposite edge channels is balanced by the Hall current in the filled Landau levels associated with the longitudinal voltage,

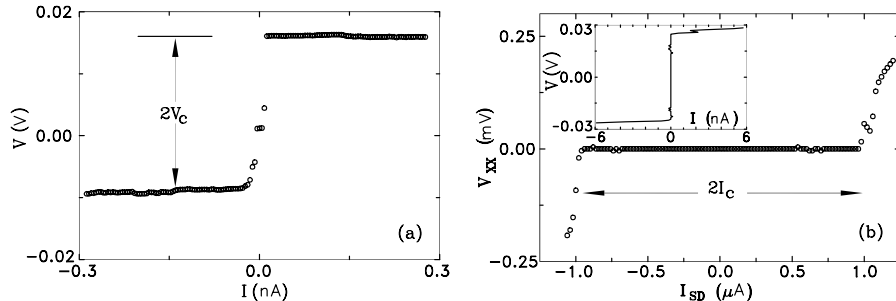


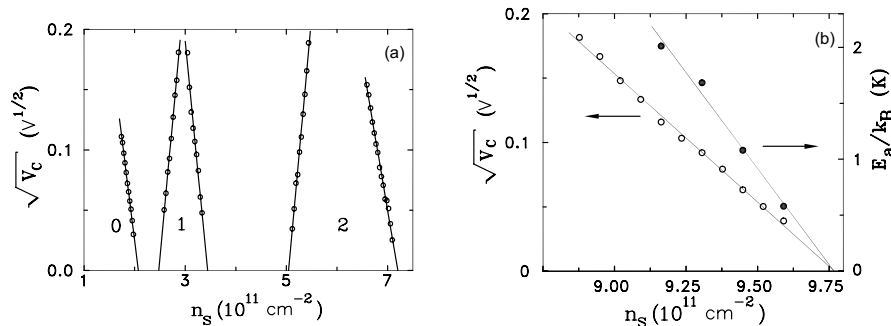
**FIGURE 1.4**

Current-voltage characteristics in a low-disordered silicon MOSFET in  $B = 12$  T at  $T \approx 25$  mK for the low-density insulating phase at  $n_s = 1.74 \times 10^{11} \text{ cm}^{-2}$  (a) and the insulating phase with  $\sigma_{xy}h/e^2 = 1$  at  $n_s = 2.83 \times 10^{11} \text{ cm}^{-2}$  (b). In (b) the measured breakdown dependence  $V_{xx}(I_{sd})$  is converted into current-voltage characteristics (inset). From Ref. [27].

$V_{xx}$ . As long as  $\sigma_{xx} \ll \sigma_{xy}$ , the quantized value of  $\sigma_{xy}$  is a factor that allows determination of  $I = \sigma_{xy}V_{xx}$  and the Hall voltage,  $V = I_{sd}/\sigma_{xy}$ , from the experimental breakdown dependence of  $V_{xx}$  on source-drain current,  $I_{sd}$ . The dependence  $V(I)$  is a current-voltage characteristic, which is equivalent to the case of Corbino geometry [27] (Fig. 1.4). Not only are the current-voltage curves similar for all insulating phases, but they also behave identically near the metal-insulator phase boundaries (Fig. 1.5(a)). The dependence of the critical voltage,  $V_c$ , on the distance from the phase boundary is close to a parabolic law [29]. The phase boundary position determined by a vanishing  $V_c$  is practically coincident with that determined by a vanishing activation energy,  $E_a$ , of electrons from the Fermi level  $E_F$  to the mobility edge,  $E_c$  (Fig. 1.5(b)). The value  $E_a$  is determined from the temperature dependence of the conduction in the linear interval of current-voltage curves, which is activated at not too low temperatures [39]; note that it transforms into variable range hopping as  $T \rightarrow 0$  (see below). The activation energy changes linearly with the distance from the phase boundary reflecting constancy of the thermodynamic density of states near the transition point (see also section 1.4). The threshold behavior of the current-voltage characteristics is caused by the breakdown in the insulating phases. The breakdown occurs when the localized electrons at the Fermi level gain enough energy to reach the mobility edge in an electric field,  $V_c/d$ , over a distance given by the localization length,  $L$  [27, 40]:

$$eV_cL/d = |E_c - E_F|, \quad (1.1)$$

where  $d$  is the corresponding sample dimension. The values  $E_a$  and  $V_c$  are related through the localization length which is temperature independent and diverges near the transition as  $L(E_F) \propto |E_c - E_F|^{-s}$  with exponent  $s$  close to unity, in agreement with the theoretical value  $s = 4/3$  in classical percolation

**FIGURE 1.5**

(a) Square root of the critical voltage as a function of electron density at the phase boundaries corresponding to  $\sigma_{xy}h/e^2 = 0, 1,$  and  $2$  in  $B = 12$  T for a low-disordered 2D electron system in silicon MOSFETs. (b) Behavior of the critical voltage and the activation energy near the phase boundary in  $B = 16$  T. From Ref. [27].

problem [41]. The value of the localization length is practically the same near all metal-insulator phase boundaries, which indicates that even quantitatively, all insulating phases are very similar. Note that since the localization length in Eq. (1.1) is small compared to the sample sizes, the phase boundary position determined by the diverging localization length refers to an infinite 2D system. As inferred from the vanishing of both  $E_a$  and  $V_c$  at the same point (see Fig. 1.5(b)), possible shifts of the mobility threshold due to finite sample dimensions are small, which justifies extrapolations to the limit of  $L \rightarrow \infty$ .

The consequences of the method include (i) as long as there occurs no dramatic change in transport properties, this excludes the pinned Wigner solid as the origin for the insulating phase at low electron densities in available samples of low-disordered silicon MOSFETs; (ii) the metal-insulator phase diagram of Fig. 1.2(a) is verified and substantiated; (iii) the existence of a metal-insulator transition in zero magnetic field is supported (see section 1.4); and (iv) the bandwidth of the extended states in the Landau levels is finite. All of these are also valid for relatively low-disordered 2D carrier systems in GaAs/AlGaAs heterostructures with a distinction that fractional quantum Hall phases are involved. Yet, the topology of the phase diagram remains unchanged including the oscillating behavior of the phase boundary that restricts the low-density insulating phase. Additional confirmation of the percolation transition to the low-density insulating phase in GaAs/AlGaAs heterostructures was obtained by studies of the high-frequency conductivity [42] and time-resolved photoluminescence of 2D electrons [43], as discussed in Ref. [28].

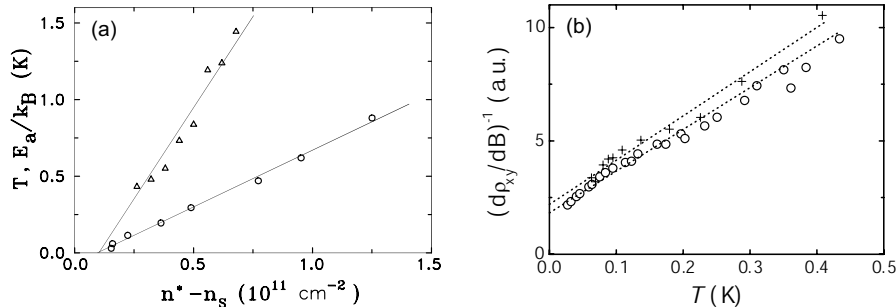
The insulating phase at low electron densities is special in what follows. Deep in the insulating state and at low temperatures the variable-range-hopping regime occurs in which the conductivity  $\sigma_{xx}$  is small compared to

its peak value [41]. In this regime it was predicted that the deviation,  $\Delta\sigma_{xy}$ , of  $\sigma_{xy}$  from its quantized value in strong magnetic fields is much smaller than  $\sigma_{xx} \propto \exp(-(T_0/T)^{1/2})$  [44]:  $\Delta\sigma_{xy} \propto \sigma_{xx}^\gamma$  with exponent  $\gamma \approx 1.5$ . A finite  $\rho_{xy}$  contrasted by diverging  $\rho_{xx}$  was found in calculations of the  $T = 0$  magneto-transport coefficients in the insulating phase with vanishing  $\sigma_{xx}$  and  $\sigma_{xy}$  [45]. Such a behavior of  $\rho_{xx}$  and  $\rho_{xy}$  indicates a special quadratic relation between conductivities:  $\sigma_{xy} \propto \sigma_{xx}^2$ . Moreover, it was shown that  $\rho_{xy}$  is close to the classical value  $(B/n_s ec)$  [46], providing arguments for the existence of a Hall insulator phase [13]. Indeed, values  $\rho_{xy}$  close to  $B/n_s ec$  were experimentally found in the low-density insulating phase. Thus, the distinction of the Hall insulator phase from the quantum Hall phases — the absence of extended states below the Fermi level — becomes evident when expressed in terms of  $\rho_{xx}$  and  $\rho_{xy}$ .

### 1.3.3 Scaling and thermal broadening

It was predicted that the localization length diverges as a power law at a single energy,  $E^*$ , which is the center of the Landau level [11]:  $L(E) \propto |E - E^*|^{-s}$ . An idea to check this prediction based on low-temperature measurements of  $\sigma_{xx}$  [47] was quickly developed to a concept of single-parameter scaling [10]. It was suggested that the magnetoresistance tensor components are functions of a single variable that is determined by the ratio of the dephasing length,  $L_d(T) \propto T^{-p/2}$  (where  $p$  is the inelastic-scattering-time exponent), and the localization length. The concept was claimed to be confirmed by measurements of temperature dependences of the peak width,  $\Delta B$ , in  $\rho_{xx}$  (or  $\sigma_{xx}$ ) and the maximum of  $d\rho_{xy}/dB$  in a highly-disordered 2D electron system in InGaAs/InP heterostructures, which yielded  $\Delta B \propto T^\kappa$ , where  $\kappa = p/2s \approx 0.4$  [48]. Later, both deviations in the power law and different exponents in the range between  $\kappa = 0.15$  and  $\kappa = 1$  were observed for other 2D carrier systems, different Landau levels, and different disorder strengths (see, e.g., Refs. [49, 50, 51, 52]). Importantly, the scaling analysis of experimental data in question is based on two unverified assumptions: (i) zero bandwidth of the extended states in the Landau levels; and (ii) constancy of the thermodynamic density of states in the scaling range. If either assumption is not valid, this may lead at least to underestimating the experimental value of exponent  $\kappa$ .

The method of vanishing activation energy and vanishing nonlinearity of current-voltage characteristics as extrapolated from the insulating phase shows that the former assumption is not justified. Also, measurements of the peak width in  $\rho_{xx}$  as a function of temperature in low-disordered silicon MOS-FETs yield a linear dependence which extrapolates as  $T \rightarrow 0$  to a finite peak width, accordingly [27] (Fig. 1.6(a)). Very similar temperature (and frequency) dependences were observed in highly-disordered 2D carrier systems in GaAs/AlGaAs heterostructures [53] and Ge/SiGe heterostructures [54]. It is noteworthy that a similar behavior is revealed if the data from the publications, which claim the observation of scaling, is plotted on a linear rather

**FIGURE 1.6**

(a) Temperature dependence of the  $\rho_{xx}$  peak width ( $n^* - n_s$ ) at half of the peak height counted from  $n^*$  corresponding to  $\nu^* = 2.5$  (circles) and the behavior of the activation energy (triangles) in a low-disordered silicon MOSFET in  $B = 14$  T. From Ref. [27]. (b) Temperature dependence of the  $\rho_{xx}$  peak width as determined by the maximum  $d\rho_{xy}/dB$  at  $\nu^* = 1.5$  in a highly-disordered 2D electron system in GaAs/AlGaAs heterostructures. Different symbols correspond to different runs. The dashed lines are linear fits to the data. Adapted from Ref. [52].

than logarithmic scale (see, e.g., Fig. 1.6(b)); finite values of the peak width as  $T \rightarrow 0$  are even more conspicuous for the data of Refs. [49, 50, 55]. The reason for the ambiguity is quite simple: within experimental uncertainty, it is difficult (especially on a logarithmic scale) to distinguish between sub-linear/superlinear fits to the data and linear fits which do not have to run through the origin. Note that attempts were made to relate the finite peak width as  $T \rightarrow 0$  to the dephasing length reaching the sample size [50, 55]; however, the suggested finite-size effect is not supported by experimental data, because in different samples with different sizes, the disorder is also different and it is the disorder, rather than the sample size, that may be responsible for the behavior of the values measured in different samples.

Although lack of data in most of the above experimental papers does not allow one to verify the validity of both assumptions, it is very likely that there is no qualitative difference between all of the discussed results. As a matter of fact, they can be described by a linear (or weakly sublinear) temperature dependence with a finite offset at  $T = 0$ . This is concurrent with the results obtained by vanishing activation energy and vanishing nonlinearity of current-voltage characteristics as extrapolated from the insulating phase. So, the single-parameter scaling is not confirmed by the experimental data which establish the finite bandwidth of the extended states in the Landau levels.

There is an alternative and simple explanation of the temperature dependence of the peak width in  $\rho_{xx}$  in terms of thermal broadening. Within percolation picture, if the activation energy  $E_a \sim k_B T$ , the conduction is of

the order of the maximum  $\sigma_{xx}$  so that the value of  $\sim k_B T$  gives a thermal shift of the effective mobility edge corresponding to the  $\sigma_{xx}$  peak width [27]. Although the concept of thermal broadening has been basically ignored in the literature in search for less trivial data interpretations, it looks as if no experimental results go beyond this favoring the concept of single-parameter scaling. Once the behavior of the localization length is not reflected by the temperature-dependent peak width in  $\rho_{xx}$ , no experimental support is provided for numeric calculations of the localization length which give a somewhat larger exponent  $s \approx 2$  compared to  $s = 4/3$  in classical percolation problem (see, e.g., Ref. [56]).

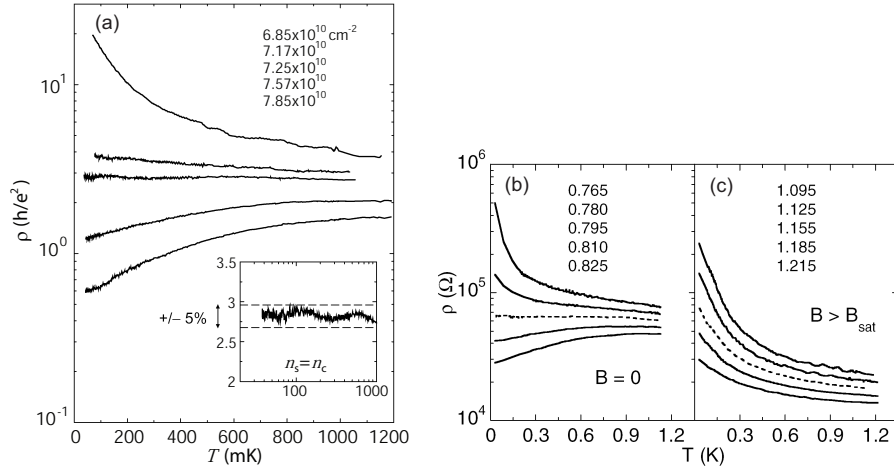
---

#### 1.4 Zero-field metal-insulator transition

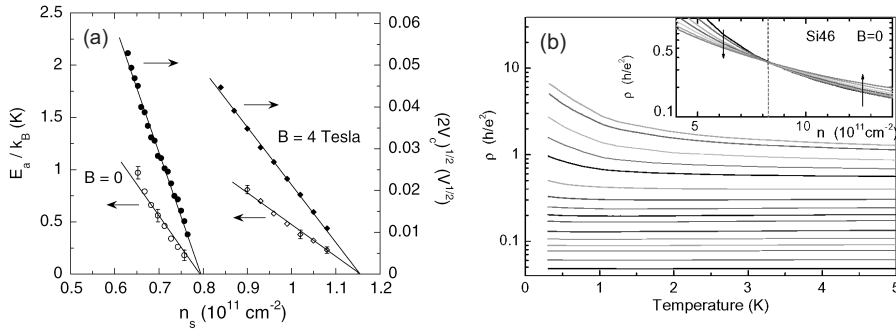
In contrast to the case of quantizing magnetic fields, no extended states are expected in zero magnetic field, at least, for weakly-interacting 2D electron systems. The criterion of vanishing activation energy and vanishing nonlinearity of current-voltage characteristics as extrapolated from the insulating phase, however, results in an opposite conclusion although it does not have absolute credibility alone. To sort it out, further support by independent experimental verifications is needed.

Another criterion is based on the analysis of the temperature dependences of the resistivity at  $B = 0$ . Provided these are strong, those with positive (negative) derivative  $d\rho/dT$  are indicative of a metal (insulator) [33, 34]; note that in the vicinity of the transition,  $\rho(T)$  dependences obey the scaling law with exponent  $\kappa \approx 1$ , which is consistent with the concept of thermal broadening/shift by the value  $\sim k_B T$  of the effective mobility edge in the insulating phase (see section 1.3.3). If extrapolation of  $\rho(T)$  to  $T = 0$  is valid, the critical point for the metal-insulator transition is given by  $d\rho/dT = 0$ . In a low-disordered 2D electron system in silicon MOSFETs, the resistivity at a certain electron density shows virtually no temperature dependence over a wide range of temperatures [33, 57] (Fig. 1.7(a)). This curve separates those with positive and negative  $d\rho/dT$  nearly symmetrically at temperatures above 0.2 K [34]. Assuming that it remains flat down to  $T = 0$ , one obtains the critical point which corresponds to a resistivity  $\rho \approx 3h/e^2$ .

Recently, these two criteria have been applied simultaneously to the 2D metal-insulator transition in low-disordered silicon MOSFETs [58, 59]. In zero magnetic field, both methods yield the same critical density  $n_c$  (Figs. 1.7(b) and 1.8(a)). Since one of the methods is temperature independent, this equivalence strongly supports the existence of a metal-insulator transition at  $T = 0$  in  $B = 0$ . This also adds confidence that the curve with zero derivative  $d\rho/dT$  will remain flat (or at least will retain finite resistivity value) down to zero

**FIGURE 1.7**

(a) Resistivity as a function of temperature at different electron densities in a low-disordered silicon MOSFET. The inset shows the middle curve on an expanded scale. From Ref. [57]. (b, c) Temperature dependence of the resistivity of a low-disordered silicon MOSFET at different electron densities near the metal-insulator transition in zero magnetic field (b) and in a parallel magnetic field of 4 T (c). The electron densities are indicated in units of  $10^{11} \text{ cm}^{-2}$ . From Ref. [58].

**FIGURE 1.8**

(a) Activation energy and square root of the threshold voltage as a function of electron density in zero magnetic field (circles) and in a parallel magnetic field of 4 T (diamonds) for the same silicon MOSFET as in Fig. 1.7(b, c). The critical densities correspond to the dashed lines in Fig. 1.7(b, c). From Ref. [58]. (b) Resistivity versus temperature in a strongly-disordered silicon MOSFET at the following electron densities: 3.85, 4.13, 4.83, 5.53, 6.23, 7.63, 9.03, 10.4, 11.8, 13.2, 16.0, 18.8, 21.6, 24.4, 30.0, and  $37.0 \times 10^{11} \text{ cm}^{-2}$ . The  $\rho(n_s)$  isotherms are shown in the inset. Adapted from Ref. [36].

temperature. Additional confirmation in favor of zero-temperature zero-field metal-insulator transition is provided by magnetic measurements [60], as described in the next section. It is argued that the metal-insulator transition in silicon samples with very low disorder potential is driven by interactions. This is qualitatively different from a localization-driven transition in more-disordered samples that occurs at appreciably higher densities.

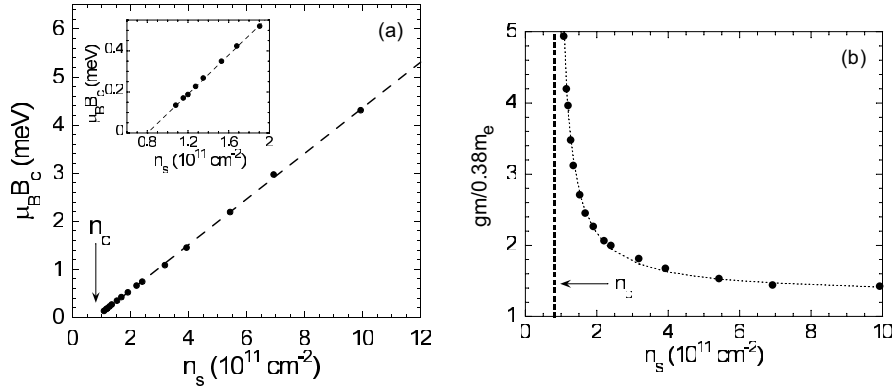
For 2D electron systems both with high disorder in zero magnetic field (see section 1.3.1) and in parallel magnetic fields, the metallic ( $d\rho/dT > 0$ ) behavior is suppressed [35, 36, 58, 61] or disappears entirely, and extrapolation of the weak  $\rho(T)$  dependences to  $T = 0$  is not justified invalidating the derivative criterion for the critical point for the metal-insulator transition (Figs. 1.7(c) and 1.8(b)). Once one of the two methods fails, it remains to be seen how to verify the conclusion as inferred from the other method. This makes uncertain the existence of a zero-temperature metal-insulator transition in 2D electron systems both with high disorder in zero magnetic field and in parallel magnetic fields.

This is noteworthy that owing to its simplicity, the derivative method is widely used for describing metallic ( $d\rho/dT > 0$ ) and insulating ( $d\rho/dT < 0$ ) temperature dependences of resistance in a restricted temperature range. To avoid confusion with metallic and insulating phases, however, one should employ alternative methods for determining the metal-insulator transition point. Such methods including a vanishing activation energy and noise measurements have been applied to highly-disordered 2D carrier systems [59, 62]. Being similar, they yield lower critical densities  $n_c$  for the metal-insulator transition compared to those obtained using formally the derivative criterion. This simply reflects the fact that the metallic ( $d\rho/dT > 0$ ) behavior is suppressed. The critical density  $n_c$ , at which the exponential divergence of the resistivity as  $T \rightarrow 0$  ends, increases naturally with disorder strength. It also increases somewhat with parallel magnetic field, saturating above a certain field, as was found in dilute silicon MOSFETs [38, 58].

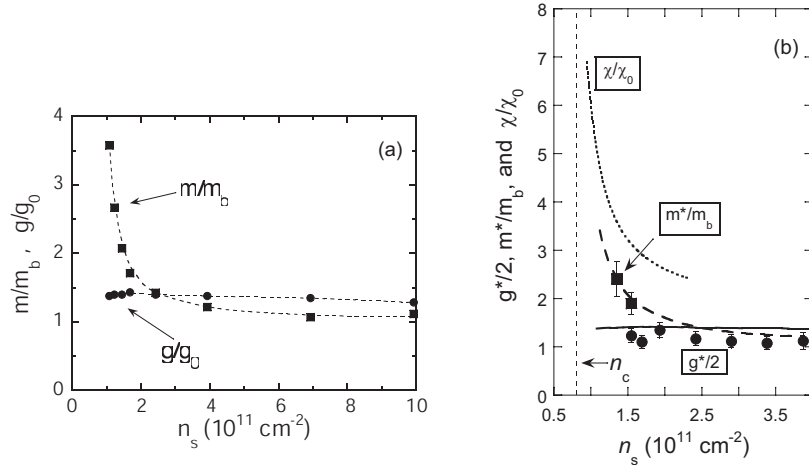
---

## 1.5 Possible ferromagnetic transition

After a strongly enhanced ratio  $gm$  of the spin and the cyclotron splittings was found at low electron densities in silicon MOSFETs [63], it became clear that the system behaves well beyond the weakly interacting Fermi liquid. It was reported that the parallel magnetic field required to produce complete spin polarization,  $B_c \propto n_s/gm$ , tends to vanish at a finite electron density  $n_\chi \approx 8 \times 10^{10} \text{ cm}^{-2}$ , which is close to the critical density  $n_c$  for the metal-insulator transition in this electron system [64] (Fig. 1.9). These findings point to a sharp increase of the spin susceptibility,  $\chi \propto gm$ , and possible ferromagnetic

**FIGURE 1.9**

(a) Dependence of the polarization field on electron density in a low-disordered silicon MOSFET. The dashed line is a linear fit. The critical density  $n_c$  is indicated. (b) The product  $gm$  versus electron density obtained from the data for  $B_c$ . From Ref. [64].

**FIGURE 1.10**

(a) The effective mass and  $g$  factor versus electron density determined from an analysis of the temperature-dependent conductivity and parallel-field magnetoresistance. The dashed lines are guides to the eye. From Ref. [66]. (b) The effective mass (squares) and  $g$  factor (circles) as a function of the electron density. The solid and long-dashed lines represent, respectively, the  $g$  factor and effective mass, previously obtained from transport measurements [66], and the dotted line is the Pauli spin susceptibility obtained by magnetization measurements in parallel magnetic fields [70]. The critical density  $n_c$  for the metal-insulator transition is indicated. From Ref. [71].

instability in dilute silicon MOSFETs. The fact that  $n_\chi$  is close to the critical density  $n_c$  indicates that the metal-insulator transition in silicon samples with very low disorder potential is a property of a clean 2D system and is driven by interactions [64]. A similar (although less pronounced) behavior was observed in other 2D carrier systems [65]. The experimental results indicated that in silicon MOSFETs it is the effective mass, rather than the  $g$  factor, that sharply increases at low electron densities [66] (Fig. 1.10(a)). They also indicated that the anomalous rise of the resistivity with temperature is related to the increased mass. The magnitude of the mass does not depend on the degree of spin polarization, which points to a spin-independent origin of the effective mass enhancement [67]. It was found that the relative mass enhancement is system- and disorder-independent and is determined by electron-electron interactions only [68].

In addition to transport measurements, thermodynamic measurements of the magnetocapacitance and magnetization of a 2D electron system in low-disordered silicon MOSFETs were performed, and very similar results for the spin susceptibility, effective mass, and  $g$  factor were obtained [69, 70, 71] (Fig. 1.10(b)). The Pauli spin susceptibility behaves critically close to the critical density  $n_c$  for the  $B = 0$  metal-insulator transition:  $\chi \propto n_s / (n_s - n_\chi)$ . This is in favor of the occurrence of a spontaneous spin polarization (either Wigner crystal or ferromagnetic liquid) at low  $n_s$ , although in currently available samples, the residual disorder conceals the origin of the low-density phase. The effective mass increases sharply with decreasing density while the enhancement of the  $g$  factor is weak and practically independent of  $n_s$ . Unlike in the Stoner scenario, it is the effective mass that is responsible for the dramatically enhanced spin susceptibility at low electron densities.

Thus, the experimental results obtained in low-disordered silicon MOSFETs indicate that on the metallic side the metal-insulator transition is driven by interactions, while on the insulating side this is still a classical percolation transition with no dramatic effects from interactions. One can consider the metal-insulator transition in the cleanest of currently available samples as a quantum phase transition, even though the problem of the competition between metal-insulator and ferromagnetic transitions is not yet resolved. It is not yet clear whether or not electron crystallization expected in the low-density limit is preceded by an intermediate phase like ferromagnetic liquid.

---

## 1.6 Outlook

Critical analysis of the available experimental data for 2D electron systems both in zero and in quantizing magnetic fields shows that consequences of the scaling theory of localization for the noninteracting 2D electrons are not con-

firmed. The main points to be addressed by theory are the problem of finite bandwidth of the extended states in the Landau levels and that of a quantum phase transition in low-disordered 2D electron systems in zero magnetic field, including the competition between metal-insulator and ferromagnetic transitions. Recently, some progress has been made in describing the behavior of low-disordered strongly interacting 2D electron systems in zero magnetic field: it has been shown that the metallic ground state can be stabilized by electron-electron interactions [9]. It is possible that it may also be necessary to take into account the electron-electron interactions to describe the quantum phase transitions that are characterized by the finite bandwidth of the extended states in the Landau levels.

The finding that in dilute 2D electron systems the spin susceptibility tends to diverge due to strong increase in the effective mass remains basically unexplained, and the particular mechanism leading to the effect remains to be seen. It is worth discussing the latest theoretical developments which are claimed to be valid for the strongly-interacting limit. According to the renormalization group analysis for multi-valley 2D systems, the effective mass dramatically increases at disorder-dependent density for the metal-insulator transition while the  $g$  factor remains nearly intact [9]. However, the prediction of disorder-dependent effective mass is in contradiction to the experiment. Besides, the results of Ref. [9] are valid only in the near vicinity of the metal-insulator transition, while the tendency of the spin susceptibility to diverge can be traced up to the densities exceeding  $n_c$  by a factor of few. In the Fermi-liquid-based model of Ref. [72], a flattening at the Fermi energy in the spectrum has been predicted that leads to a diverging effective mass. Still, the expected dependence of the effective mass on temperature is not confirmed by the experimental data. The strong increase of the effective mass has been obtained (in the absence of the disorder) by solving an extended Hubbard model using dynamical mean-field theory [73]. This is consistent with the experiment, especially taking into account that the relative mass enhancement has been experimentally found to be independent of the level of the disorder. The dominant increase of  $m$  near the onset of Wigner crystallization follows also from an alternative description of the strongly-interacting electron system beyond the Fermi liquid approach (see, *e.g.*, Ref. [74]).

On the experimental side, the progress in the fabrication of increasingly high mobility Si, Si/SiGe, and GaAs-based devices will open the possibility of probing the intrinsic properties of clean 2D electron systems at still lower densities, where electron-electron interactions are yet stronger and, presumably, the previously observed behaviors will be yet more pronounced. Moreover, as high mobility devices made with other semiconductors become available, further tests of the universality of the observed phenomena will add to our knowledge of the quantum phase transitions in two dimensions.

---

## References

- [1] E. Wigner, *Phys. Rev.* **46**, 1002 (1934).
- [2] E. C. Stoner, *Rep. Prog. Phys.* **11**, 43 (1946).
- [3] L. D. Landau, *Sov. Phys. JETP* **3**, 920 (1957).
- [4] B. Tanatar and D. M. Ceperley, *Phys. Rev. B* **39**, 5005 (1989).
- [5] C. Attaccalite, S. Moroni, P. Gori-Giorgi, and G. B. Bachelet, *Phys. Rev. Lett.* **88**, 256601 (2002).
- [6] E. Abrahams, P. W. Anderson, D. C. Licciardello, and T. V. Ramakrishnan, *Phys. Rev. Lett.* **42**, 673 (1979).
- [7] B. L. Altshuler, A. G. Aronov, and P. A. Lee, *Phys. Rev. Lett.* **44**, 1288 (1980).
- [8] A. M. Finkelstein, *Sov. Phys. JETP* **57**, 97 (1983); *Z. Phys. B* **56**, 189 (1984); C. Castellani, C. Di Castro, P. A. Lee, and M. Ma, *Phys. Rev. B* **30**, 527 (1984).
- [9] A. Punnoose and A. M. Finkelstein, *Science* **310**, 289 (2005).
- [10] A. M. M. Pruisken, *Phys. Rev. Lett.* **61**, 1297 (1988).
- [11] S. V. Iordansky, *Solid State Commun.* **43**, 1 (1982); T. Ando, *J. Phys. Soc. Jpn.* **52**, 1740 (1983); H. Aoki, *J. Phys. C* **16**, 1893 (1983).
- [12] D. E. Khmel'nitskii, *Phys. Lett. A* **106**, 182 (1984); R. B. Laughlin, *Phys. Rev. Lett.* **52**, 2304 (1984).
- [13] S. A. Kivelson, D. H. Lee, and S. C. Zhang, *Phys. Rev. B* **46**, 2223 (1992).
- [14] D. E. Khmel'nitskii, *Helv. Phys. Acta* **65**, 164 (1992).
- [15] Y. E. Lozovik and V. I. Yudson, *JETP Lett.* **22**, 11 (1975).
- [16] B. I. Halperin, *Phys. Rev. B* **25**, 2185 (1982).
- [17] K. von Klitzing, G. Dorda, and M. Pepper, *Phys. Rev. Lett.* **45**, 494 (1980).
- [18] *The Quantum Hall Effect*, Ed. by R. E. Prange and S. M. Girvin (Springer-Verlag, 1987).
- [19] H. Levine, S. B. Libby, and A. M. M. Pruisken, *Phys. Rev. Lett.* **51**, 1915 (1983).
- [20] M. Büttiker, *Phys. Rev. B* **38**, 9375 (1988).

- [21] R. B. Laughlin, Phys. Rev. B **23**, 5632 (1981); A. Widom and T. D. Clark, J. Phys. D **15**, L181 (1982).
- [22] V. T. Dolgoplov, A. A. Shashkin, N. B. Zhitenev, S. I. Dorozhkin, and K. von Klitzing, Phys. Rev. B **46**, 12560 (1992).
- [23] E. Y. Andrei, G. Deville, D. C. Glattli, F. I. B. Williams, E. Paris, and B. Etienne, Phys. Rev. Lett. **60**, 2765 (1988).
- [24] M. D'Iorio, V. M. Pudalov, and S. G. Semenchinsky, Phys. Lett. A **150**, 422 (1990).
- [25] M. B. Santos, Y. W. Suen, M. Shayegan, Y. P. Li, L. W. Engel, and D. C. Tsui, Phys. Rev. Lett. **68**, 1188 (1992).
- [26] A. A. Shashkin, G. V. Kravchenko, and V. T. Dolgoplov, JETP Lett. **58**, 220 (1993).
- [27] A. A. Shashkin, V. T. Dolgoplov, and G. V. Kravchenko, Phys. Rev. B **49**, 14486 (1994).
- [28] A. A. Shashkin, V. T. Dolgoplov, G. V. Kravchenko, M. Wendel, R. Schuster, J. P. Kotthaus, R. J. Haug, K. von Klitzing, K. Ploog, H. Nickel, and W. Schlapp, Phys. Rev. Lett. **73**, 3141 (1994).
- [29] V. T. Dolgoplov, G. V. Kravchenko, A. A. Shashkin, and S. V. Kravchenko, Phys. Rev. B **46**, 13303 (1992).
- [30] S. V. Kravchenko, W. Mason, J. E. Furneaux, and V. M. Pudalov, Phys. Rev. Lett. **75**, 910 (1995).
- [31] M. Hilke, D. Shahar, S. H. Song, D. C. Tsui, and Y. H. Xie, Phys. Rev. B **62**, 6940 (2000).
- [32] I. Glazman, C. E. Johnson, and H. W. Jiang, Phys. Rev. Lett. **74**, 594 (1995).
- [33] M. P. Sarachik and S. V. Kravchenko, Proc. Natl. Acad. Sci. USA **96**, 5900 (1999).
- [34] E. Abrahams, S. V. Kravchenko, and M. P. Sarachik, Rev. Mod. Phys. **73**, 251 (2001); S. V. Kravchenko and M. P. Sarachik, Rep. Prog. Phys. **67**, 1 (2004).
- [35] Y. Hanein, U. Meirav, D. Shahar, C. C. Li, D. C. Tsui, and H. Shtrikman, Phys. Rev. Lett. **80**, 1288 (1998); M. Y. Simmons, A. R. Hamilton, M. Pepper, E. H. Linfield, P. D. Rose, D. A. Ritchie, A. K. Savchenko, and T. G. Griffiths, Phys. Rev. Lett. **80**, 1292 (1998).
- [36] V. M. Pudalov, G. Brunthaler, A. Prinz, and G. Bauer, cond-mat/0103087.

- [37] V. T. Dolgoplov, G. V. Kravchenko, and A. A. Shashkin, *JETP Lett.* **55**, 140 (1992).
- [38] V. T. Dolgoplov, G. V. Kravchenko, A. A. Shashkin, and S. V. Kravchenko, *JETP Lett.* **55**, 733 (1992).
- [39] C. J. Adkins, S. Pollitt, and M. Pepper, *J. Phys. C* **37**, 343 (1976).
- [40] D. G. Polyakov and B. I. Shklovskii, *Phys. Rev. B* **48**, 11167 (1993).
- [41] B. I. Shklovskii and A. L. Efros, *Electronic Properties of Doped Semiconductors* (Springer, New York, 1984).
- [42] Y. P. Li, PhD thesis, Princeton University, 1994.
- [43] I. V. Kukushkin and V. B. Timofeev, *Sov. Phys. Usp.* **36**, 549 (1993).
- [44] K. I. Wysokinski and W. Brenig, *Z. Phys. B* **54**, 11 (1983).
- [45] O. Viehweger and K. B. Efetov, *J. Phys. Condens. Matter* **2**, 7049 (1990).
- [46] S. C. Zhang, S. Kivelson, and D. H. Lee, *Phys. Rev. Lett.* **69**, 1252 (1992).
- [47] H. Aoki and T. Ando, *Phys. Rev. Lett.* **54**, 831 (1985).
- [48] H. P. Wei, D. C. Tsui, M. A. Paalanen, and A. M. M. Pruisken, *Phys. Rev. Lett.* **61**, 1294 (1988).
- [49] V. T. Dolgoplov, A. A. Shashkin, B. K. Medvedev, and V. G. Mokerov, *Sov. Phys. JETP* **72**, 113 (1991).
- [50] S. Koch, R. J. Haug, K. von Klitzing, and K. Ploog, *Phys. Rev. Lett.* **67**, 883 (1991).
- [51] J. Wakabayashi, M. Yamane, and S. Kawaji, *J. Phys. Soc. Jpn.* **58**, 1903 (1989); T. Wang, K. P. Clark, G. F. Spencer, A. M. Mack, and W. P. Kirk, *Phys. Rev. Lett.* **72**, 709 (1994).
- [52] H. P. Wei, S. Y. Lin, D. C. Tsui, and A. M. M. Pruisken, *Phys. Rev. B* **45**, 3926 (1992).
- [53] N. Q. Balaban, U. Meirav, and I. Bar-Joseph, *Phys. Rev. Lett.* **81**, 4967 (1998); D. Shahar, M. Hilke, C. C. Li, D. C. Tsui, S. L. Sondhi, J. E. Cunningham, and M. Razeghi, *Solid State Commun.* **107**, 19 (1998).
- [54] M. Hilke, D. Shahar, S. H. Song, D. C. Tsui, Y. H. Xie, and D. Monroe, *Phys. Rev. B* **56**, R15545 (1997).

- [55] W. Li, C. L. Vicente, J. S. Xia, W. Pan, D. C. Tsui, L. N. Pfeiffer, and K. W. West, *Phys. Rev. Lett.* **102**, 216801 (2009).
- [56] B. Huckestein, *Rev. Mod. Phys.* **67**, 357 (1995).
- [57] S. V. Kravchenko and T. M. Klapwijk, *Phys. Rev. Lett.* **84**, 2909 (2000).
- [58] A. A. Shashkin, S. V. Kravchenko, and T. M. Klapwijk, *Phys. Rev. Lett.* **87**, 266402 (2001).
- [59] J. Jaroszyński, D. Popović, and T. M. Klapwijk, *Phys. Rev. Lett.* **89**, 276401 (2002).
- [60] A. A. Shashkin, *Phys. Usp.* **48**, 129 (2005).
- [61] A. A. Shashkin, E. V. Deviatov, V. T. Dolgoplov, A. A. Kapustin, S. Anissimova, A. Venkatesan, S. V. Kravchenko, and T. M. Klapwijk, *Phys. Rev. B* **73**, 115420 (2006).
- [62] S. Bogdanovich and D. Popović, *Phys. Rev. Lett.* **88**, 236401 (2002); R. Leturcq, D. L'Hote, R. Tourbot, C. J. Mellor, and M. Henini, *Phys. Rev. Lett.* **90**, 076402 (2003).
- [63] S. V. Kravchenko, A. A. Shashkin, D. A. Bloore, and T. M. Klapwijk, *Solid State Commun.* **116**, 495 (2000).
- [64] A. A. Shashkin, S. V. Kravchenko, V. T. Dolgoplov, and T. M. Klapwijk, *Phys. Rev. Lett.* **87**, 086801 (2001).
- [65] X. P. A. Gao, A. P. Mills Jr., A. P. Ramirez, L. N. Pfeiffer, and K. W. West, *Phys. Rev. Lett.* **89**, 016801 (2002); J. Zhu, H. L. Stormer, L. N. Pfeiffer, K. W. Baldwin, and K. W. West, *Phys. Rev. Lett.* **90**, 056805 (2003); T. Okamoto, M. Ooya, K. Hosoya, and S. Kawaji, *Phys. Rev. B* **69**, 041202 (2004).
- [66] A. A. Shashkin, S. V. Kravchenko, V. T. Dolgoplov, and T. M. Klapwijk, *Phys. Rev. B* **66**, 073303 (2002).
- [67] A. A. Shashkin, M. Rahimi, S. Anissimova, S. V. Kravchenko, V. T. Dolgoplov, and T. M. Klapwijk, *Phys. Rev. Lett.* **91**, 046403 (2003).
- [68] A. A. Shashkin, A. A. Kapustin, E. V. Deviatov, V. T. Dolgoplov, and Z. D. Kvon, *Phys. Rev. B* **76**, 241302(R) (2007).
- [69] V. S. Khrapai, A. A. Shashkin, and V. T. Dolgoplov, *Phys. Rev. Lett.* **91**, 126404 (2003).
- [70] A. A. Shashkin, S. Anissimova, M. R. Sakr, S. V. Kravchenko, V. T. Dolgoplov, and T. M. Klapwijk, *Phys. Rev. Lett.* **96**, 036403 (2006).

- [71] S. Anissimova, A. Venkatesan, A. A. Shashkin, M. R. Sakr, S. V. Kravchenko, and T. M. Klapwijk, *Phys. Rev. Lett.* **96**, 046409 (2006).
- [72] V. A. Khodel, J. W. Clark, and M. V. Zverev, *Europhys. Lett.* **72**, 256 (2005).
- [73] S. Pankov and V. Dobrosavljević, *Phys. Rev. B* **77**, 085104 (2008).
- [74] B. Spivak and S. A. Kivelson, *Phys. Rev. B* **70**, 155114 (2004).